Proceedings of the ASME 38th International Conference on Ocean, Offshore and Arctic Engineering
OMAE2019
June 9-14, 2019, Glasgow, Scotland

OMAE2019-96321

COMPUTATIONAL METHODS FOR MOVING AND DEFORMING OBJECTS IN EXTREME WAVES

Arthur E.P. Veldman*
Henk Seubers

Bernoulli Institute
University of Groningen
P.O. Box 407, 9700 AK Groningen
The Netherlands
{a.e.p.veldman, h.seubers}@rug.nl

Matin Hosseini
Xing Chang
Peter R. Wellens

Department of Ship Hydromechanics
Delft University of Technology
Mekelweg 2, 2628 CD Delft
The Netherlands
p.r.wellens@tudelft.nl

Peter van der Plas
Joop Helder

MARIN
P.O. Box 28, 6700AA Wageningen
The Netherlands
{p.v.d.plas, j.helder}@marin.nl

ABSTRACT

Wave forces can form a serious threat to offshore platforms and ships. The damage produced by these forces of nature jeopardizes their operability as well as the well-being of their crews. Similar remarks apply to coastal defense systems. To develop the knowledge needed to safely design these constructions, in close cooperation with MARIN and the offshore industry the numerical simulation method ComFLOW is being developed. So far, its development was focussed on predicting wave loads (green water, slamming) on fixed structures, and for those applications the method is already being used successfully by the offshore industry. Often, the investigated object (ship, floating platform) is dynamically moving under the influence of these wave forces, and its hydrodynamic loading depends upon the position of the object with respect to the oncoming waves. Predicting the position (and deformation) of the body is an integral part of the (scientific and engineering) problem. The paper will give an overview of the algorithmic developments necessary to describe the abovementioned physical phenomena. In particular attention will be paid to fluid-solid body and fluid-structure interaction and non-reflecting outflow boundary conditions. Several illustrations including validation, will demonstrate the prediction capabilities of the simulation method.

*Address all correspondence to this author.

1 INTRODUCTION

Waves and currents can induce large forces and stresses on sea-going ships and offshore constructions (production and offloading platforms, mooring systems, wind turbine farms) that have to operate under extreme weather conditions [1]. E.g. in heavy storms, wave and ship motions can become so large that solid amounts of seawater, called 'green water', flow over the deck, thus threatening the safety and operability of the ship. The amount of shipped water obviously depends on the phase between ship and wave motion, and hence on the preceeding wave group and its interaction with the ship dynamics. The same holds for slamming impacts against a ship's bow. As a special case, free fall lifeboats (Fig. 1) face these challenges when a ship or platform needs to be evacuated.

In the past, these violent flow phenomena were mainly studied experimentally, and there is a growing need for a numerical simulation tool capable of predicting in detail the hydrodynamic loads due to slamming and green water; see e.g. [2–4]. Tools based on e.g. linear potential flow theory or shallow-water theory are hardly capable of predicting such events to an acceptable level of accuracy [5]. As the physical phenomena accompanying extreme events are both highly non-linear and highly dispersive due to the occurring wave steepness, they require new vevels of modeling to predict the water flow and its hydrodynamic loads. Thus, in recent years, tools based on the Navier–Stokes equations

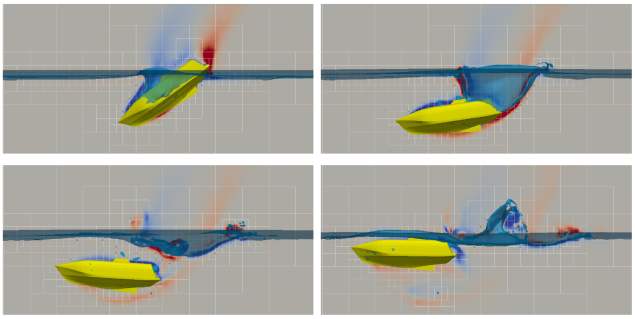

FIGURE 1. SIMULATED SNAPSHOTS OF A FREE-FALL LIFE BOAT.

have become availablefor large-scale complex free-surface flow problems, thanks to novel numerical algorithms and the increase in computer power [6–8]. For an overview of basic Navier–Stokes methods for free-surface flow we refer to [9]. Some recent applications, including the interaction with solid/elastic bodies, can be found in [10–16].

The ComMotion project also uses a hydrodynamic flow model based on the Navier–Stokes equations for simulating the steep waves near and around (interactively) moving and deforming structures. In this paper, we will present the main physical and (innovative) numerical ingredients of the project:

- Interactively moving bodies.
- Hydroelasticity.
- Absorbing boundary conditions incorporating current.
- Experimental validation.

For reliable load predictions in these examples, it is necessary to determine the position and dynamics of the objects as part of the flow simulation. The project makes this major step by extending the simulation method to interactively moving and deforming objects in extreme waves. The underlying numerical coupling approach will receive much attention in this paper. It is based on the quasi-simultaneous method developed four decades ago in the airplane industry [17], and recently re-discovered in the (offshore) FSI community [18, 19]. Also, attention is paid to numerical absorbing outflow boundary conditions in the presence of current. The new developments will be illustrated with a number of maritime applications.

2 MODELLING

2.1 Flow model

Incompressible, turbulent fluid flow can be modelled by means of the Navier–Stokes equations.

$$M\mathbf{u} = 0, \qquad \frac{\partial \mathbf{u}}{\partial t} + C(\mathbf{u})\mathbf{u} + Gp - V\mathbf{u} = \mathbf{f}. \tag{1}$$

Here M is the divergence operator, which describes conservation of mass. Conservation of momentum is based on the convection operator $C(\mathbf{u})\mathbf{v} \equiv \nabla(\mathbf{u}\otimes\mathbf{v})$, the pressure gradient operator $G = \nabla$, the viscous diffusion operator $V(\mathbf{u}) \equiv \nabla\cdot\nu\nabla\mathbf{u}$ and a forcing term $\mathbf{f}$. The kinematic viscosity is denoted by ν. Turbulence is modelled by means of large-eddy simulation (LES) using a low-dissipation QR-model as formulated by Verstappen [20] and refined by Rozema [21–23]. For its use in maritime applications, see [24, 25].

The evolution of the free water surface is described by an adapted and improved version of the Volume-of-Fluid method (VOF) introduced in [6] and [26]. Specifically, use will be made of the ComFLOW simulation method, developed at the University of Groningen in cooperation with the Technical University of Delft and MARIN. It is described in full detail in a series of PhD theses [27–34].

The computational grid is chosen rectangular; the simplicity of the grid gives an easy geometric framework in which the position and slope of the water surface can be accurately described. The free-surface location is indicated by a Volume-of-Fluid [6] function, which is reconstructed by Youngs' PLIC method [32, 35] and advanced by a local height function [27, 32].

Bodies can move and deform through the fixed Cartesian grid, with their position described in a cut-cell fashion by edge and volume apertures, as is done for non-moving objects [36] (see also [37, 38]). Local grid refinement [39] can be applied near the body and in other interesting flow regions.

The Navier–Stokes equations (1) are discretized on a staggered grid [40]. The second-order finite-volume discretization of the continuity equation at the 'new' time level $\cdot^{n+1}$ is given by

$$\mathsf{M}_0\mathbf{u}^{n+1} = -\mathsf{M}_\Gamma\mathbf{u}_\Gamma^{n+1}, \tag{2}$$

where M_0 acts on the interior of the domain and M_Γ acts on the boundaries of the domain. Skew-symmetric convection $\mathsf{C}(\mathbf{u}_h)$ and symmetric diffusion V are discretized explicitly in time. In this exposition, for simplicity reasons the first-order forward Euler time integration will be used. In the actual calculations, a second-order Adams–Bashforth method is being applied.

The discrete momentum equation can be formulated as

$$\mathbf{u}^{n+1} = \tilde{\mathbf{u}} - \delta t\,\Omega^{-1}\mathsf{G}\mathsf{p}^{n+1}, \tag{3}$$

where $\tilde{\mathbf{u}}$ is an abbreviation given by

$$\tilde{\mathbf{u}} = \mathbf{u}^n + \delta t\,\Omega^{-1}[-\mathsf{C}(\mathbf{u}^n)\mathbf{u}^n + \mathsf{V}\mathbf{u}^n + \mathbf{f}]. \tag{4}$$

Here, the diagonal matrix Ω contains the geometric size of the control volumes. This discretization does not produce artificial diffusion and convectively preserves the energy of the flow

[22, 41]. Also, the discrete gradient operator and the divergence operator are each other's negative transpose, i.e. $\mathsf{G} = -\mathsf{M}_0^T$, mimicking the analytic symmetry $\nabla = -(\nabla\cdot)^T$. In this way, also the work done by the pressure vanishes discretely.

Imposing discrete mass conservation (2) at the new time level, substitution of (3) results in a discrete Poisson equation for the pressure:

$$\delta t\, \mathsf{M}_0 \Omega^{-1} \mathsf{G} \mathsf{p}^{n+1} = \mathsf{M}_0 \tilde{\mathbf{u}} + \mathsf{M}_\Gamma \mathbf{u}_\Gamma^{n+1}. \tag{5}$$

Here Γ is the boundary of the fluid domain where boundary conditions involving the velocity are prescribed; it includes the fluid-solid interface Γ_{FS}.

In the coupling analysis to be presented below, it is convenient to abbreviate the above Navier–Stokes solution process into a formal, abstract notation as

$$\mathsf{M}_{\mathrm{ad}} \ddot{\mathbf{d}}_{\Gamma_{\mathrm{FS}}} = -\mathbf{f}_{\Gamma_{\mathrm{FS}}}. \tag{6}$$

Here, $\mathbf{d}_{\Gamma_{\mathrm{FS}}}$ is the displacement of the fluid-solid interface Γ_{FS}, whereas $\mathbf{f}_{\Gamma_{\mathrm{FS}}}$ represents the forces (stresses) along the interface excerted by the object towards the fluid (hence the minus-sign). In this short-hand notation, M_{ad} can be regonized as the so-called added-mass operator, which governs the relation between the motion of an immersed object and the reactive forces excerted by the fluid.

2.2 Structural model

For simplicity in this study, the structure is selected to be a one dimensional Euler–Bernoulli beam. Assuming a constant cross section $A = TW$ for the beam (thickness T and width W), its equation of motion is

$$\rho_s A \frac{\partial^2 d}{\partial t^2} + EI \frac{\partial^4 d}{\partial s^4} = f, \tag{7}$$

with appropriate initial and boundary conditions. Here, s denotes a coordinate along the beam, d the beam deformation, ρ_s the beam density, E Young's modulus, I the second moment of inertia and f the load per unit length of the beam. In principle, the structural model can be replaced by other models (e.g. with structural damping), as it is approached as a 'black-box' model wih no invasive action required. The coupling behaviour will remain similar to the issues discussed in this paper.

In our simulations, the structural response is modeled with a finite element method. Omitting the technical details, the resulting discrete set of equations can be written in the form

$$\mathsf{M}_{\mathrm{eb}} \ddot{\mathbf{d}}_{\Gamma_{\mathrm{FS}}} + \mathsf{K}_{\mathrm{eb}} \mathbf{d}_{\Gamma_{\mathrm{FS}}} = \mathbf{f}_{\Gamma_{\mathrm{FS}}}, \tag{8}$$

where M_{eb} is the discrete mass operator and K_{eb} the discrete stiffness operator. The temporal integration of the structure equations is performed by means of the generalized-α method [42].

2.3 Fluid-solid coupling conditions

The coupling relations along the fluid-solid interface Γ_{FS} consist of two relations. The kinematic condition states that the (local) motion of the interface on both sides matches:

$$\text{kinematic:} \qquad \mathbf{u} = \frac{\partial d}{\partial t}\mathbf{n} \qquad \text{on } \Gamma_{\mathrm{FS}} \tag{9}$$

The dynamic condition expresses (local) equilibrium of stresses along the fluid-solid interface:

$$\text{dynamic:} \qquad \overline{\overline{\sigma}}_f \cdot \mathbf{n} = \overline{\overline{\sigma}}_s \cdot \mathbf{n} \qquad \text{on } \Gamma_{\mathrm{FS}} \tag{10}$$

Note that this equilibrium in principle contains both normal and tangential stresses. In the simulations below, only the (normal) pressure forces are included here as the viscosity is low.

3 NUMERICAL COUPLING

A traditional hierarchical numerical coupling method may not be sufficient, as its stability depends on the ratio between body mass versus added mass (the amount of liquid that 'moves with' the body). Note that this ratio can vary widely, depending on geometry and motion of the body. Therefore, a more powerful unsteady quasi-simultaneous coupling method has been developed.

Traditional weak (hierarchical) coupling methods, with information exchange once per time step, are only numerically stable within a restricted range of mass (or stiffness) ratios. If the application covers a larger range, one has to resort to strong (simultaneous) coupling; compare fluid-structure interaction [43]. Usually, some form of subcycling within each time step is applied, where information is exchanged at the 'hearts' of the numerical algorithms (like in a monolithic code). However, when 'black-box' commercial codes are being used this is unlikely to be feasible, as access to the internal core of their algorithms is usually not possible. The approach that we have developed here allows for a 'black-box' structural solver, and only requires access to the internal iterative loops of the fluid flow solver (ComFLOW). The extension of the method to the coupling of two 'black-box' solvers is feasible, e.g. [19], but will not be pursued in this paper.

Fortunately, it is not necessary to perform a *fully* simultaneous coupling. A good approximation of one of the two submodels is sufficient to be fully intertwined with the other submodel.

The difference between the approximation and the original submodel can be dealt with in the traditional, weak fashion. Such a coupling is called *quasi-simultaneous*, and was introduced in a steady, aerodynamic context in the late 1970s [17, 44, 45]. In time-integration terms: the bulk of the interaction is treated implicitly, the remaining part explicitly. Numerical stability of this approach requires that, roughly spoken, the implicit part contains at least 'half of the physics', which is a very weak requirement. The essential step is that the equations approximating the other submodel, such as an elastic wall model, are considered boundary conditions for the fluid flow equations. In particular, they will show up as a boundary condition in the pressure Poisson equation.

Recently, in the literature similar methods have been presented for the FSI problems that we are treating here. We mention the quasi-monolithic method as developed independently in the group of Visonneau at the Ecole Centrale in Nantes, e.g. [13, 15, 18]. Besides the remarkably similar name of the method, it also makes use of a simple model for one of the domains which is solved simultaneously with the equations in the other domains. The difference is that an approximation for the fluid added mass is solved together with the structural equations, whereas we solve an approximation for the structure together with the fluid-flow equations. As the fluid added mass is less easily approximated than the structural mass, the quasi-monolithic method often requires Aitken under-relaxation for stability [12, 15].

3.1 Elastic body coupling

The quasi-simultaneous procedure can be explained for the general case of an elastic body - the solid body case fits in. The deformation of the elastic body is governed by Eq. (8). The equation governing the fluid flow has been schematized in (6). Thus, in principle we have two equations with two unknowns along the fluid-solid interface Γ_{FS}. Because these equations contain both $\ddot{\mathbf{d}}$ and $\mathbf{d}$ (we refrain from using the subscripts $\cdot_{\Gamma_{\mathrm{FS}}}$ from now on), first a discrete time integration is carried out. Thereafter, the discrete version of the hierarchically coupled problem at the new time level can be denoted as

$$\text{Elastic body} \qquad \left(\frac{\mathsf{M}_{\mathrm{eb}}}{\delta t^2}+\mathsf{K}_{\mathrm{eb}}\right)\mathbf{d}^{k+1}=\mathbf{f}^{k}+\ldots, \tag{11}$$

$$\text{Fluid} \qquad \mathbf{f}^{k+1}=-\frac{\mathsf{M}_{\mathrm{ad}}}{\delta t^2}\mathbf{d}^{k+1}. \tag{12}$$

Here, M_{eb} denotes the discrete elastic body mass operator, while K_{eb} is the discrete elastic body stiffness operator; compare (8). The contributon from the previous time steps is omitted in view of clarity; it is just an inhomogeneous term in the right-hand side, which is not relevant for the convergence of the subiterations per time step.

Matrices M_{eb} and K_{eb} can be simultaneously diagonalized as $\mathsf{Q}^T\mathsf{M}_{\mathrm{eb}}\mathsf{Q}=\mathsf{I}$ and $\mathsf{Q}^T\mathsf{K}_{\mathrm{eb}}\mathsf{Q}=\Lambda$. Here, Q contains the normalized elastic body eigenvectors with eigenvalues Λ. In this way, the elastic body dynamics (11) can be rewritten as

$$\text{Elastic body} \qquad \mathsf{Q}^{-T}\left(\frac{\mathsf{I}}{\delta t^2}+\Lambda\right)\mathsf{Q}^{-1}\mathbf{d}^{k+1}=\mathbf{f}^{k}. \tag{13}$$

The displacement $\mathbf{d}^{k+1}$ can be eliminated from the system of equations (12) and (13), after which the iterative process can be written as

$$\mathbf{f}^{k+1}=-\mathsf{M}_{\mathrm{ad}}\mathsf{Q}(\mathsf{I}+\delta t^2\Lambda)^{-1}\mathsf{Q}^T\mathbf{f}^{k}. \tag{14}$$

For small enough δt, the amplification factor simplifies to $\mathsf{M}_{\mathrm{ad}}\mathsf{Q}\mathsf{Q}^T$, where $\mathsf{Q}\mathsf{Q}^T$ has the dimension of $1/kg$. For a solid body with 6 DOF, the latter can be replaced by the inverse solid-body mass $\mathsf{M}_{\mathrm{sb}}^{-1}$.

In the Appendix it is shown that the lower modes are most delicate, as they correspond with the largest fluid added mass. Therefore we take care that these modes are treated more simultaneous. Thus we construct an approximation of the full elastic equations, called *interaction law*, built from the lowest elastic modes of the structure. In other words, we define an approximation $\widetilde{\mathsf{Q}}$ by only retaining the first few eigenvectors. These correspond with the largest eigenvalues in Λ, i.e. the lowest natural frequencies, which will be collected in $\widetilde{\Lambda}$.

Proceeding in this way, the proposed interaction law reads

$$\mathbf{d}^{k+1}-\widetilde{\mathsf{Q}}\left(\frac{1}{\delta t^2}+\widetilde{\Lambda}\right)^{-1}\widetilde{\mathsf{Q}}^T\mathbf{f}^{k+1}= \left\{\mathsf{Q}\left(\frac{1}{\delta t^2}+\Lambda\right)^{-1}\mathsf{Q}^T-\widetilde{\mathsf{Q}}\left(\frac{1}{\delta t^2}+\widetilde{\Lambda}\right)^{-1}\widetilde{\mathsf{Q}}^T\right\}\mathbf{f}^{k}.$$

Letting $\delta t\to 0$, i.e. studying zero-stability, and combining with the fluid-flow model (12), the quasi-simultaneous iterative process can be formulated as

$$\mathbf{f}^{k+1}=-(\mathsf{M}_{\mathrm{ad}}^{-1}+\widetilde{\mathsf{Q}}\widetilde{\mathsf{Q}}^T)^{-1}(\mathsf{Q}\mathsf{Q}^T-\widetilde{\mathsf{Q}}\widetilde{\mathsf{Q}}^T)\mathbf{f}^{k}, \tag{15}$$

which can be compared with (14) for $\delta t=0$. Clearly, if all of the modes are incorporated into the interaction law, the spectral radius will become zero and the method simultaneously solves the fluid with the 'exact' body.

3.2 Implementation

The interaction law is a relation between the pressure and the local velocity of the body surface. This relation can be substituted in the right-hand side of the discrete mass equation (2).

Thus it becomes a boundary condition for the discrete Poisson equation. It can be shown that the latter retains it favourable numerical properties (symmetric, negative definite), such that its iterative solution can proceed as before.

3.3 Elastic body: tank with membrane bottom

In order to assess the performance of the quasi-simultaneous approach for different mass ratios, a test case has been designed in which this ratio can be varied. Also, the physical contents of the interaction law has been varied.

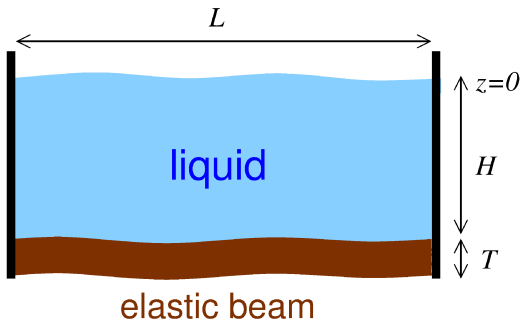

FIGURE 2. SCHEMATIC OF THE FIRST TEST CASE; THE DOMAIN WITH FREE-SURFACE FLOW ON TOP AND FLEXIBLE BEAM AT THE BOTTOM

At the bottom of a rectangular container ($1.0 \times 0.1 \times 0.5\,\mathrm{m}^3$) filled with 50 kg of water, a flexible beam is placed as illustrated in Fig. 2. The mass of the beam is varied between 1 kg and 50 kg; its module of elasticity is 1 MPa. The interaction law is made out of truncated structural modes; the number of modes dictates its accuracy.

Cases with mass ratio 1 and 50 are presented, where the number of included modes is increased in order of relevance. Figure 3 shows the convergence history during the first time step. The effect of the number of modes in the interaction law can be inferred. For a small added mass ratio one mode suffices, but for the more difficult mass ratio 50 it is profitable to include more modes in the interaction law. This behaviour is perfectly in line with the stability analysis in the Appendix.

3.4 Solid body: CALM buoy

The second case is a validation against model tests of a CALM buoy (Fig. 4) in a shallow water basin at MARIN [46]. These tests include the freely decaying motion of the buoy after being released from a given position into calm water. This allows us to compare the simulated and measured natural periods as well as the amount of hydrodynamic damping. The buoy in its default configuration has been modelled as a cylinder with a diameter of 12 m and a height of 6.5 m.

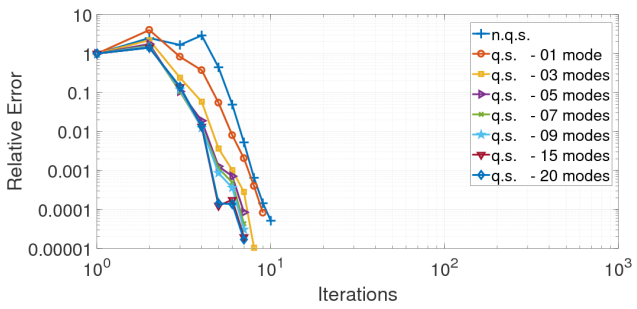

(a) Convergence history for added mass ratio 1

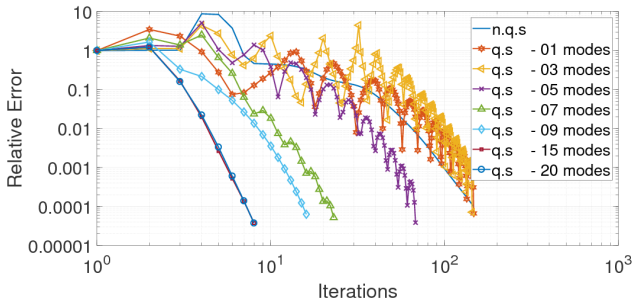

(b) Convergence history for added mass ratio 50

FIGURE 3. CONVERGENCE HISTORY FOR THE FIRST TIME STEP FOR AN INCREASING NUMBER OF INCLUDED MODES (q.s. = quasi-simultaneous; n.q.s. = non-q.s.)

The simulation has been performed at different grids, with approximately 6, 10 and 18 cells per cylinder diameter. The results for heave motion are shown in Fig. 5. Using the approach of Eça et al. [47], the numerical uncertainty has been assessed from these three grids and also indicated. The resulting uncertainty was found quite small, whereas it is understandable that for later times in the simulation the uncertainty increases. The validation of the simulations was carried by a comparison with the experiments at MARIN and also indicated in Fig. 5. The period as well as damping of the heave motion are found well-predicted. Note that the small offset in the heave motion can be decreased by slightly tuning (decreasing) the buoy's mass parameter in the simulations.

4 ABSORBING BOUNDARY CONDITIONS

In the CALM-buoy simulations, the computational domain has to be restricted to a finite region. Therefore, one has to take care that no numerical reflections from these artificial domain boundaries enter the physical region of interest. To minimize these reflections a new type of absorbing boundary conditions (ABC) has been developed, which can adapt itselves to the passing waves [31, 32, 48]. To enlarge its application domain, the effect of current (in arbitrary direction) has been included. In 2D,

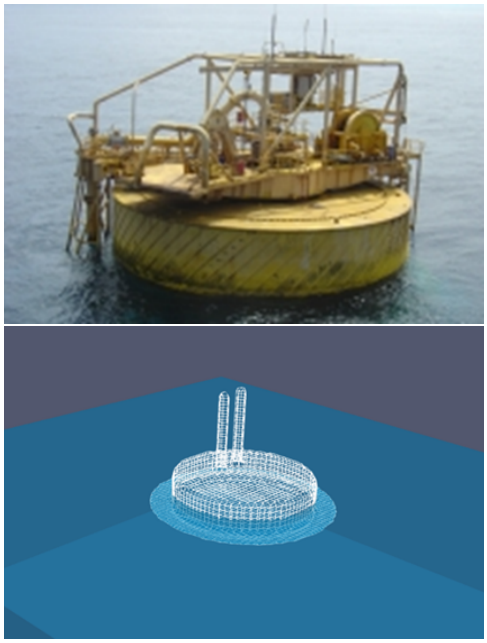

FIGURE 4. A CALM BUOY AT SEA (TOP) AND ITS GEOMETRICAL REPRESENTATION IN THE SIMULATIONS (BOTTOM)

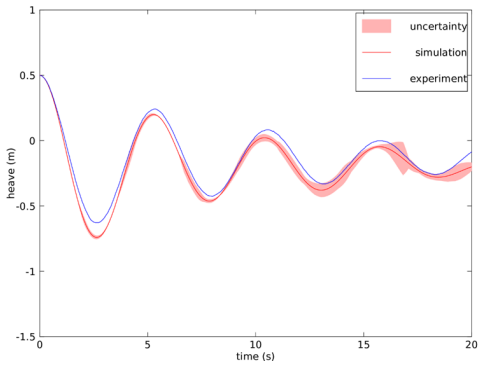

FIGURE 5. HEAVE MOTIONS OF A FREE-FLOATING CALM BUOY IN SIMULATION AND EXPERIMENT

Peregrine [49] already studied the effect of current on the dispersion relation. In 3D the dispersion relation involving current $\mathbf{U}$ reads, using the abbreviations $k = |\mathbf{k}|$ and $U_k \equiv \mathbf{U}\cdot\mathbf{k}/k$,

$$\omega_{\pm} = U_k + c_{k0} \quad \text{with} \quad c_{k0} = \sqrt{gh}\sqrt{\frac{\tanh(kh)}{kh}}. \tag{16}$$

The ABC is basically of Sommerfeld type, which in 3D reads as

$$\left[\cos\alpha\left(\frac{\partial}{\partial t} + \mathbf{U}\cdot\nabla\right) + c_{k0}\frac{\partial}{\partial n}\right]\phi_w = 0, \tag{17}$$

where α is the angle between the wave $\mathbf{k}$ and the normal $\mathbf{n}$. This new condition lets waves with wave number $\mathbf{k}$ pass freely; it is not unique. Further, ϕ_w is the wave component of the potential, which is reformulated in terms of pressure p and velocity $\mathbf{u}$, using the unsteady Bernoulli equation, as

$$\frac{\partial\phi_w}{\partial t} + \mathbf{U}\cdot\nabla\phi_w = -\left(\frac{p}{\rho} - \frac{p}{\rho}\bigg|_{\text{atm}}\right) - g(z - z_0) \text{ and } \nabla\phi_w = \mathbf{u} - \mathbf{U}.$$

This results in a relation between p and $\mathbf{u}$ which is used as a boundary condition to the pressure Poisson equation, similar to the interaction law for fluid-structure interaction that we discussed above. The phase speed c_{k0} is replaced by a Padé approximation, with the unknown wave number $\mathbf{k}$ found from the local solution [32, 48].

The performance of this ABC is tested by studying the reflections of irregular waves under current at an outflow boundary. The geometry is chosen 2D. A short domain of length 10 m and depth 10 m has been chosen, with a current of 1 m/sec. Figure 6 (top) shows the incoming wave spectrum, with a peak period of 6 sec and significant wave height 2 m. The reflections have been calculated by comparing with a much larger domain, such that the reflections have not yet reached the domain of interest. The reflected wave spectrum is shown in Fig. 6 (bottom) When keeping the frequency ω constant, (16) predicts that the wave number of opposing waves is enlarged (Doppler shift): the waves become shorter due to the current. This is visible in the shift of the wave number of the reflected waves. A theoretical reflection coefficient can be calculated analytically (not shown here) and is plotted for comparison.

Figure 7 shows a simulation of an oscillating sphere, with prescribed motion, which generates outgoing waves. A current is present, running in diagonal direction through the domain. The current makes the radiating circles no longer concentric. The domain has been kept rather small, in order to study reflections at the boundaries. The figure clearly shows no visible irregularities near the domain boundaries, showing the potential of the new ABC.

5 CONCLUSION

Several of the newly-developed ingredients of the ComFLOW simulation method have been presented. Firstly, a quasi-simultaneous numerical coupling method has been presented. It can handle large added-mass ratios efficiently and can also be extended to cover the coupling with elastically-deforming objects. The lower elastic modes are found the most 'tricky' and can be 'tamed' by including them in the interaction law. Secondly, ComFLOW's absorbing boundary condition which adjusts itself to the oncoming waves has been extended to cover the influence of current. Several examples of verification and validation have been included.

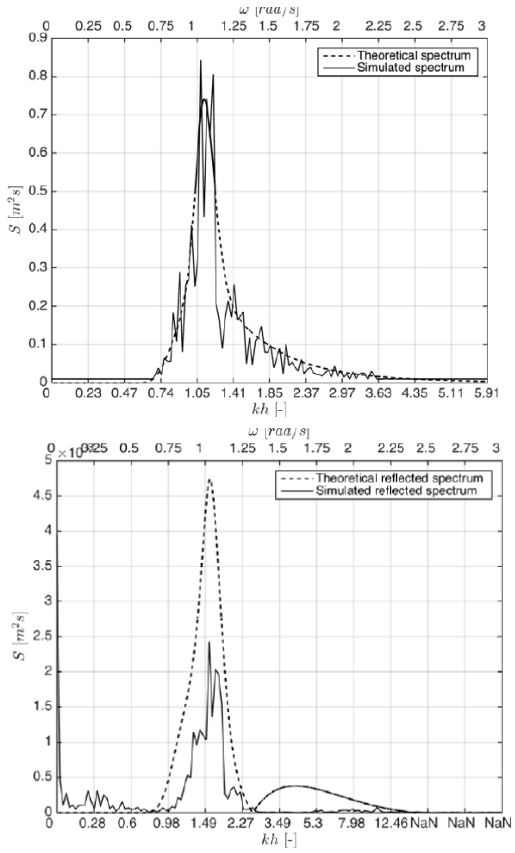

FIGURE 6. IRREGULAR WAVE SPECTRUM (TOP) AND REFLECTIONS (BOTTOM). NOTE THE CHANGE IN WAVE NUMBER.

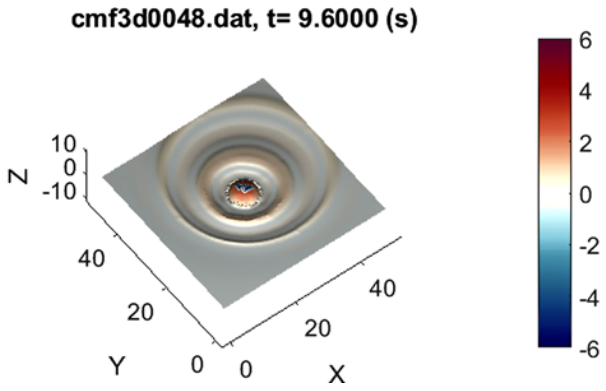

FIGURE 7. OSCILLATING BUOY IN A CURRENT, GENERATING NON-CONCENTRIC WAVES)

6 ACKNOWLEDGMENTS

This work is part of the research programme Maritime2013 with project number 13267 which is (partly) financed by the Netherlands Organisation for Scientific Research (NWO).

REFERENCES

[1] Haver, S., 2000. "Evidences of the existence of freak waves". In Rogue Waves 2000, Proc. of Int. Workshop, Ifremer, ed., pp. 129–140.

[2] Faltinsen, O. M., 1999. *Sea Loads on Ships and Offshore Structures*. Cambridge University Press.

[3] Buchner, B., 2002. "Green water on ship-type offshore structures". PhD Thesis, University of Delft, Delft, The Netherlands, November.

[4] Molin, B., and Ferziger, J., 2003. "Hydrodynamique des structures offshore". *Appl. Mech. Rev.,* ***56***, p. B29.

[5] Tsai, W., and Yue, D. K. P., 1996. "Computation of nonlinear free-surface flows". *Ann. Rev. Fluid Mech.,* ***28***, pp. 249–278.

[6] Hirt, C. W., and Nichols, B. D., 1981. "Volume of fluid (VOF) method for the dynamics of free boundaries". *J. Comput. Phys.,* ***39***, pp. 201–25.

[7] Rider, W. J., and Kothe, D. B., 1998. "Reconstructing volume tracking". *J. Comput. Phys.,* ***141***, pp. 112–152.

[8] Yabe, T., Xiao, F., and Utsumi, T., 2001. "The constrained interpolation profile method for multiphase analysis". *J. Comput. Phys.,* ***169***, pp. 556–593.

[9] Osher, S. J., and Tryggvason (eds.), G., 2001. "Special issue on 'Computational Methods for Multiphase Flows"'. *J. Comput. Phys.,* ***169***, pp. 249–759.

[10] Menter, F., Sharkey, P., Yakubov, S., and Kuntz, M., 2006. "Overview of fluid-structure coupling in ansys-cfx". In Proc. 25th Int. Conf. Offshore Mech. Arctic Eng., pp. 579–585.

[11] Constantinides, Y., Yu, W., and Holmes, S., 2011. "VIV prediction of a truss spar pull-tube array using CFD". In Proc. 30th Int. Conf. Ocean, Offshore Arctic Eng., pp. 637–643.

[12] Durand, M., Leroyer, A., Lothodé, C., Hauville, F., Visonneau, M., Floch, R., and Guillaume, L., 2014. "Fsi investigation on stability of downwind sails with an automatic dynamic trimming". *Ocean Engineering,* ***90***, pp. 129–139.

[13] Gross, D., 2015. "New quasi-monolithic method to solve dynamic fluid-structure interaction problems on membranes". In Textiles composites and inflatable structures VII: proc. VII Int. Conf. on Textile Composites and Inflatable Structures, Barcelona, Spain. 19-21 October, 2015, CIMNE, pp. 344–355.

[14] Oliveira, D., Santiago, A., and Rigueiro, C., 2016. "Fluid structure interaction in offshore environment". In Proc. 5th Int. Conf. on Integrity-Reliability-Failure, J. S. Gomes and S. Meguid, eds. Paper ref: 6258.

[15] Yvin, C., Leroyer, A., Visonneau, M., and Queutey, P., 2018. "Added mass evaluation with a finite-volume solver

for applications in fluid–structure interaction problems solved with co-simulation". *J. Fluids Struct.,* ***81***, pp. 528–546.

[16] Naseri, A., Lehmkuhl, O., Gonzalez, I., Bartrons, E., Pérez-Segarra, C. D., and Oliva, A., 2018. "A semi-implicit coupling technique for fluid–structure interaction problems with strong added-mass effect". *J. Fluids Struct.,* ***80***, pp. 94–112.

[17] Veldman, A. E. P., 1981. "New, quasi-simultaneous method to calculate interacting boundary layers". *AIAA J.,* ***19***, pp. 79–85.

[18] Durand, M., 2012. "Interaction fluide-structure souple et l egere, application aux voiliers". PhD thesis, Ecole Centrale de Nantes (ECN).

[19] Degroote, J., 2013. "Partitioned simulation of fluid-structure interaction". *Arch. Comput. Meth. Eng.,* ***20***(3), pp. 185–238.

[20] Verstappen, R., 2011. "When does eddy viscosity damp subfilter scales sufficiently?". *J. Sci. Comput.,* ***49***(1), pp. 94–110.

[21] Rozema, W., 2015. "Low-dissipation methods and models for the simulation of turbulent subsonic flow". PhD thesis, University of Groningen.

[22] Rozema, W., Verstappen, R. W. C. P., Kok, J. C., and Veldman, A. E. P., 2018. "Low-dissipation simulation methods and models for turbulent subsonic flow". *Arch. Comput. Meth. Eng.* DOI: 10.1007/s11831-018-09307-7.

[23] Abkar, M., Bae, H. J., and Moin, P., 2016. "Minimum-dissipation scalar transport model for large-eddy simulation of turbulent flows". *Physical Review Fluids,* ***1***(4), p. 041701.

[24] van der Heiden, H. J. L., Veldman, A. E. P., Luppes, R., van der Plas, P., Helder, J., and Bunnik, T., 2015. "Turbulence modeling for free-surface flow simulations in offshore applications". In Proc. 34th Int. Conf. Ocean, Offshore Arctic Eng. OMAE2015. paper OMAE2015-41078.

[25] Veldman, A. E. P., Luppes, R., van der Plas, P., van der Heiden, H. J. L., Helder, J., and Bunnik, T., 2015. "Turbulence modeling for locally-refined free-surface flow simulations in offshore applications". In Proc. Int. Symp. Offshore Polar Eng. ISOPE2015. paper ISOPE2015-TPC-0282.

[26] Kleefsman, K. M. T., Fekken, G., Veldman, A. E. P., Iwanowski, B., and Buchner, B., 2005. "A Volume-of-Fluid based simulation method for wave impact problems". *J. Comput. Phys.,* ***206***, pp. 363–393.

[27] Gerrits, J., 2001. "Dynamics of liquid-filled spacecraft". PhD thesis, University of Groningen, The Netherlands.

[28] Fekken, G., 2004. "Numerical simulation of free-surface flow with moving objects". PhD Thesis, University of Groningen, The Netherlands.

[29] Kleefsman, K. M. T., 2005. "Water impact loading on offshore structures - a numerical study". PhD thesis, University of Groningen, The Netherlands.

[30] Wemmenhove, R., 2008. "Numerical simulation of two-phase flow in offshore environments". PhD Thesis, University of Groningen, The Netherlands.

[31] Wellens, P. R., 2012. "Wave simulation in truncated domains for offshore applications". PhD Thesis, Technical University Delft, The Netherlands.

[32] Düz, B., 2015. "Wave generation, propagation and absorption in CFD simulations of free surface flows". PhD thesis, Technical University Delft.

[33] van der Plas, P., 2017. "Local grid refinement for free-surface flow simulations". PhD thesis, University of Groningen.

[34] van der Heiden, H. J. L., 2019. "Modelling viscous effects in offshore flow problems - a numerical study". PhD thesis, University of Groningen.

[35] Youngs, D. L., 1987. An interface tracking method for a 3d Eulerian hydrodynamics code. Technical Report AWRE/44/92/35, Atomic Weapons Research Establishment.

[36] Dröge, M., and Verstappen, R., 2005. "A new symmetry-preserving Cartesian-grid method for computing flow past arbitrarily shaped objects". *Int. J. Numer. Meth. Fluids,* ***47***, pp. 979–985.

[37] Cheny, Y., and Botella, O., 2010. "The LS-STAG method; a new immersed boundary/level-set method for the computation of incompressible viscous flows in complex moving geometries with good conservation properties". *J. Comput. Phys.,* ***229***, pp. 1043–1076.

[38] Gu, H. B., Causon, D. M., Mingham, C. G., and Qian, L., 2013. "Development of a free surfcae flow solver for the simulation of wave/body interactions". *Eur. J. Mech. B/Fluids,* ***38***, pp. 1–17.

[39] Veldman, A. E. P., van der Plas, P., Seubers, H., Helder, J., and Lam, K.-W., 2018. "Adaptive grid refinement for two-phase offshore applications". In Proc. 37th Int. Conf. Ocean, Offshore Arctic Eng. OMAE2018. paper OMAE2018-77309.

[40] Harlow, F. H., and Welch, J. E., 1965. "Numerical calculation of time-dependent viscous incompressible flow of fluid with free surface". *Phys. Fluids,* ***8***, pp. 2182–2189.

[41] Verstappen, R. W. C. P., and Veldman, A. E. P., 2003. "Symmetry-preserving discretization of turbulent flow". *J. Comput. Phys.,* ***187***, pp. 343–368.

[42] Chung, J., and Hulbert, G. M., 1992. "A time integration algorithm for structural dynamics with improved numerical dissipation: the generalized-α method". *J. Appl. Mech.,* ***60***(2), August, pp. 371–375.

[43] Causin, P., Gerbau, J. F., and Nobile, F., 2005. "Added-mass effect in the design of partitioned algorithms for fluid-structure problems". *Comput. Methods Appl. Mech. Engr.,* ***194***, pp. 4506–4527.

[44] Cebeci, T., and Cousteix, J., 1999. *Modeling and Computation of Boundary-Layer Flows*. Springer.
[45] Veldman, A. E. P., 2009. "A simple interaction law for viscous-inviscid interaction". *J. Eng. Math.,* ***65***, pp. 367–383.
[46] Bunnik, T. H. J., and van Doeveren, A. G., 2008. CALM buoy model tests. Tech. Rep. report 18378-3-BT, MARIN.
[47] Eça, L., and Hoekstra, M., 2006. "Discretization uncertainty estimation based on a least squares version of the grid convergence index". In Proc. 2nd Workshop on CFD Uncertainty Analysis, Instituto Superior Tecnico, Lisbon.
[48] Düz, B., Borsboom, M. J. A., Wellens, P. R., Veldman, A. E. P., and Huijsmans, R. H. M., 2017. "An absorbing boundary condition for free-surface water waves". *Comput. Fluids,* ***156***, pp. 562–578.
[49] Peregrine, D. H., 1976. "Interaction of water waves and currents". *Advances in Applied Mechanics.,* ***16***, pp. 9–117.

APPENDIX: NUMERICAL COUPLING STABILITY

Consider a partially-filled open tank with a flexible bottom (thickness T and width W). The free surface is $z=0$, whereas the bottom of the tank is at $z=-H$ (Fig. 2). The flow is assumed to be potential flow. The pressure satisfying an atmospheric boundary condition at the free surface reads:

$$p=\rho_f \sinh(kz)\, e^{\mathrm{i}kx}\, e^{\mathrm{i}\omega t} \quad \Rightarrow \quad \frac{\partial p}{\partial z}=\rho_f k \cosh(kz)\, e^{\mathrm{i}kx}\, e^{\mathrm{i}\omega t}, \qquad (18)$$

where ρ_f is the density of the fluid. The relation between potential Φ and pressure p is given by a linearized unsteady Bernoulli equation valid throughout the fluid domain: $\rho_f \frac{\partial \Phi}{\partial t}+p=0$. At the bottom, it can be formulated for the fundamental solutions as

$$\rho_f \frac{\partial^2 d}{\partial t^2}+\left.\frac{\partial p}{\partial z}\right|_{z=-H}=0 \quad \Rightarrow \quad p=-\frac{\tanh(kH)}{k}\frac{\partial^2 d}{\partial t^2}, \qquad (19)$$

where $d\equiv \int_t \partial\Phi/\partial z|_{z=-H}\,\mathrm{d}t$ is the displacement of the bottom. Eq. (19) basically is the relation between pressure and displacement from the fluid dynamics. The 'twin' relation from the structural dynamics was already given in Eq. (7) above as an Euler–Bernoulli beam.

The stability analysis in discrete time of Eqs. (19) and (7) assumes Fourier behaviour $e^{\mathrm{i}kx}$ in x-direction, and fulfillment of the boundary conditions in z-direction as above. The second-order time derivative is approximated, as usual for hyperbolic equations, via a backward formula in time. In the weak coupling method, the step from $t^{(n)}\rightarrow t^{(n+1)}$ can be denoted as

$$p^{(n)}=\rho_f \frac{\tanh(kH)}{k}\,\frac{d^{(n)}-2d^{(n-1)}+d^{(n-2)}}{\delta t^2},$$

$$\rho_s TW\frac{d^{(n+1)}-2d^{(n)}+d^{(n-1)}}{\delta t^2}+EIk^4 d^{(n+1)}=-Wp^{(n)}.$$

Elimination of the pressure, and using the notation from Table 1, leads to

$$\mu_s\left(d^{(n+1)}-2d^{(n)}+d^{(n-1)}\right)+\delta t^2\kappa_k d^{(n+1)}= -\mu_{f,k}\left(d^{(n)}-2d^{(n-1)}+d^{(n-2)}\right).$$

$\mu_s\equiv\rho_s TW$	mass of solid per unit x-length
$\mu_f\equiv\rho_f HW$	mass of fluid per unit x-length
$\mu_{f,k}\equiv\mu_f\frac{\tanh(kH)}{kH}$	modal mass of fluid per unit x-length
$\kappa_k\equiv EIk^4$	modal stiffness parameter

TABLE 1. Notation for (modal) mass and stiffness. Observe that $0<\mu_{f,k}\leq\mu_f$, while $\mu_{f,k}\sim 1/k$ for $k\rightarrow\infty$.

Setting $d^{(n)}=\lambda^n$, the characteristic equation of the above difference relation can be formulated as

$$\mu_s(\lambda^3-2\lambda^2+\lambda)+\delta t^2\kappa_k\lambda^3=-\mu_{f,k}(\lambda^2-2\lambda+1). \qquad (20)$$

Some calculus shows that there are two physical roots

$$\lambda_{1,2}=1\pm\mathrm{i}\,\delta t\sqrt{\frac{\kappa_k}{\mu_s+\mu_{f,k}}}+\mathcal{O}(\delta t^2),$$

and one parasitic root

$$\lambda_3=-\frac{\mu_{f.k}}{\mu_s}+\mathcal{O}(\kappa_k\,\delta t^2).$$

The two physical roots of (20) correspond with oscillatory motion; their amplitude is $|\lambda_{1,2}|=1+\mathcal{O}(\delta t^2)$, hence they are numerically zero stable, i.e. 'harmless'. The parasitic root λ_3 is the one which can give the problems that we are tackling. We can conclude from the behaviour of the modal added mass $\mu_{f,k}\sim 1/k$ that higher wave numbers give less problems.